Chapter 5
Orientation Effects and Anisotropy of Properties in 0–3 Composites

A piezo-active composite with 0–3 connectivity represents a system of isolated inclusions (either FC or ferroelectric SC) in a large matrix that may be either a polymer or FC. As follows from the analysis of papers on 0–3 ferroelectric based composites, in the last decades the FC/polymer composites have attracted widespread interest as they are attractive for piezo-technical applications [1–3]. Of an independent interest are the SC/polymer [3] and SC/FC [3–5] composites with various 0–3 connectivity patterns. The effective electromechanical properties of 0–3 composites comprising one or two ferroelectric components have been studied using experimental [6–12] and theoretical [3, 13–19] methods. In these studies the microgeometry of the composite, electromechanical properties of its components, poling conditions of the composite sample, etc. have been discussed to show specific advantages of the 0–3 composite materials. The role of the microgeometrical factor in forming the electromechanical properties at a transition from the 0–3 connectivity pattern to related patterns [3, 18] is also of interest in the context of the prediction of the performance of the composite materials.

Chapter 5 is concerned with the study of the effective properties, their anisotropy and orientation effects in piezo-active 0–3 composites. We discuss results on the 0–3 composites and show routes for improving some parameters of these materials to make them more suitable for a variety of piezo-technical applications.

5.1 Composites Based on Ferroelectric Ceramics

5.1.1 Role of Microgeometry in Forming the Large Anisotropy of Properties

The 0–3 $PbTiO_3$-type FC/epoxy resin composite is an example of a modern piezo-active material prepared by electric-field structuring [12]. The microstructure and electromechanical properties of this composite are attained due to use of

V. Yu. Topolov et al., *Piezo-Active Composites*,
Springer Series in Materials Science 185, DOI: 10.1007/978-3-642-38354-0_5,

dielectrophoresis for the structural modification. When using this process, a dispersion of FC particles embedded in a liquid polymer or pre-polymer is exposed to a moderate electric field, that leads to the formation of chain-like structures in a polymer matrix. After a solidification of the polymer medium, these structures remain stable in the composite sample [12]. An analysis of the composite microstructure suggests that this material is characterised by 0–3 connectivity, and the shape of the FC inclusions therein approaches a spheroidal shape.

The effective electromechanical properties of the 0–3 FC/polymer composite with spheroidal inclusions can be predicted on the basis of different averaging methods and procedures (see, e.g., papers [3, 13–15, 17, 19]) where full sets of electromechanical constants were predicted. We follow a model [19] that has first been applied to 0–3 composites based on the $(Pb_{1-x}Ca_x)TiO_3$ FC [3] with a large piezoelectric anisotropy. In this model the shape of each inclusion (Fig. 5.1, component 1) is spheroidal and obeys Eq. (3.27) relative to the axes of the rectangular co-ordinate system $(X_1X_2X_3)$. The semi-axes of each spheroidal inclusion are $a_1 = a_2$ and a_3, and the aspect ratio is $\rho = a_1/a_3$. A remanent polarisation vector of each inclusion is $\boldsymbol{P}_r^{(1)} \uparrow\uparrow OX_3$, and the OX_3 axis is the poling axis of the composite sample as a whole. A regular distribution of spheroidal inclusions is considered so that these inclusions would occupy sites of a simple tetragonal lattice with unit-cell vectors parallel to the OX_j axes. Electrical conductivities $\gamma^{(1)}$ of the FC and $\gamma^{(2)}$ of the polymer are linked with an inequality $\gamma^{(2)} \geq \gamma^{(1)}$, and surface charges caused by the ferroelectric polarisation are fully screened by free carriers coming to the interfaces in the composite sample.

The components of the composite are characterised by sets of elastic moduli $c_{ab}^{(n),E}$, piezoelectric coefficients $e_{ij}^{(n)}$ and dielectric permittivities $\varepsilon_{pp}^{(n),\xi}$, where $n = 1$ is related to FC (inclusions), and $n = 2$ is related to polymer (the surrounding matrix). The effective electromechanical properties determined in the long-wavelength limit [3] depend on the volume fraction m of FC and the aspect ratio ρ.

The calculation procedure is based on the EFM and Eshelby's concept of spheroidal inclusions [3, 17, 19, 20], and this concept is regarded [3, 17] as a variant of the self-consistent scheme for the calculation of effective constants of the piezoactive composite. A matrix of the effective electromechanical properties of the 0–3 composite is determined as $||C^*|| = ||C^*(m, \rho)||$ in accordance with (4.22) and is

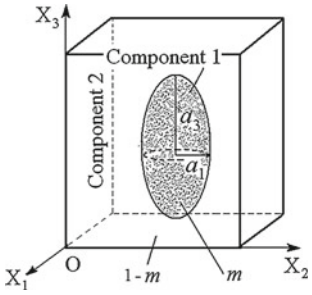

Fig. 5.1 Schematic of the 0–3 composite with spheroidal inclusions. $(X_1X_2X_3)$ is the rectangular co-ordinate system, a_i are semi-axes of the spheroid, m is the volume fraction of component 1, and $1 - m$ is the volume fraction of component 2

represented in the general form (4.1). The electromechanical properties are characterised by $||C^{(1)}||$ (FC) and $||C^{(2)}||$ (polymer), and these matrices have the form similar to that shown in (4.1).

As is known from experimental data [3, 19], important features of the $PbTiO_3$-type FCs are three positive piezoelectric coefficients $e_{ij}^{(1)}$ (Table 5.1) and a large anisotropy of the piezoelectric coefficients $d_{3j}^{(1)}$ at room temperature, i.e., an inequality $d_{33}^{(1)}/|d_{31}^{(1)}| \gg 1$ holds, and signs of $d_{3j}^{(1)}$ obey (4.3). Examples of the calculated volume-fraction dependence of effective parameters of the 0–3 composite based on the modified $PbTiO_3$ FC are shown in Fig. 5.2. To avoid some distinctions between the properties of the $PbTiO_3$-type FC from experimental work [12] and the modified $PbTiO_3$ FC [3] involved in our calculations, we introduce normalised dielectric permittivity $\beta_\varepsilon = \varepsilon_{33}^{*\sigma}/\varepsilon_{33}^{(1),\sigma}$ and normalised piezoelectric coefficients $\beta_d = d_{33}^*/d_{33}^{(1)}$ and $\beta_g = g_{33}^*/g_{33}^{(1)}$. Good agreement between the experimental and calculated volume-fraction dependences of β_ε is observed at aspect ratios $\rho = 0.13 - 0.19$ (Fig. 5.2a). The structured 0–3 FC/polymer composite can be represented as an aggregate of prolate inclusions in a matrix, with the aforementioned aspect ratios of these inclusions. A similar microstructure of the 0–3 composite is observed in experimental work [12]. The volume-fraction dependence of β_ε for an unstructured 0–3 composite with the same components may be approximated by pieces of curves at $\rho \approx 0.32 - 0.50$ (Fig. 5.2b). It is obvious that a transition from the prolate FC inclusion (oriented along the poling direction) to the spherical (or oblate) FC inclusion leads to the creation of obstacles for poling the composite sample and leads to poor piezoelectric properties.

Among the piezoelectric coefficients d_{3j}^*, e_{3j}^*, g_{3j}^*, and h_{3j}^* of the studied 0–3 composite, g_{31}^* and g_{33}^* are the most sensitive [19, 21] to changes in the volume fraction m and the aspect ratio ρ of the SC inclusions. For example, at $\rho = 0.01-0.20$, ratios $\max \beta_g \approx 3 - 10$ and $\min g_{31}^*/g_{31}^{(1)} \approx 9 - 40$ are attained. A difference between the aforementioned ratios is related to the key role of the system of the prolate FC inclusions in forming the anisotropic piezoelectric response of the 0–3 composite (Fig. 5.1). Due to this system, the volume-fraction dependence of β_d and β_g (Fig. 5.2c, d) resembles the volume-fraction dependence of the piezoelectric coefficients d_{33}^* and g_{33}^*, respectively, in the 1–3$PbTiO_3$-type FC/polymer composite [3, 18]. An advantage of the studied 0–3 composite is the relatively large $\max\beta_g$ values near the volume fraction $m = 0.1$ at various aspect ratios ρ (Fig. 5.2d), and this performance is concerned with a favourable balance of elastic moduli $c_{ab}^{(n),E}$ of components and with a relatively low dielectric permittivity $\varepsilon_{33}^{*\sigma}$ of the composite at $0 < m \leq 0.1$. As follows from (1.12), $\varepsilon_{33}^{*\sigma}$ strongly influences both g_{33}^* and β_g of the composite. Examples of behaviour of two anisotropy factors, ζ_d^* from (4.24) and

$$\zeta_e^* = e_{33}^*/e_{31}^* = (2d_{31}^* c_{13}^{*E} + d_{33}^* c_{33}^{*E})/[d_{31}^*(c_{11}^{*E} + c_{12}^{*E}) + d_{33}^* c_{13}^{*E}], \tag{5.1}$$

are shown in Fig. 5.2e, f, respectively. It is seen that ζ_e^* is varied in a wider range, and this variation is due to the influence of elastic properties of the FC and polymer

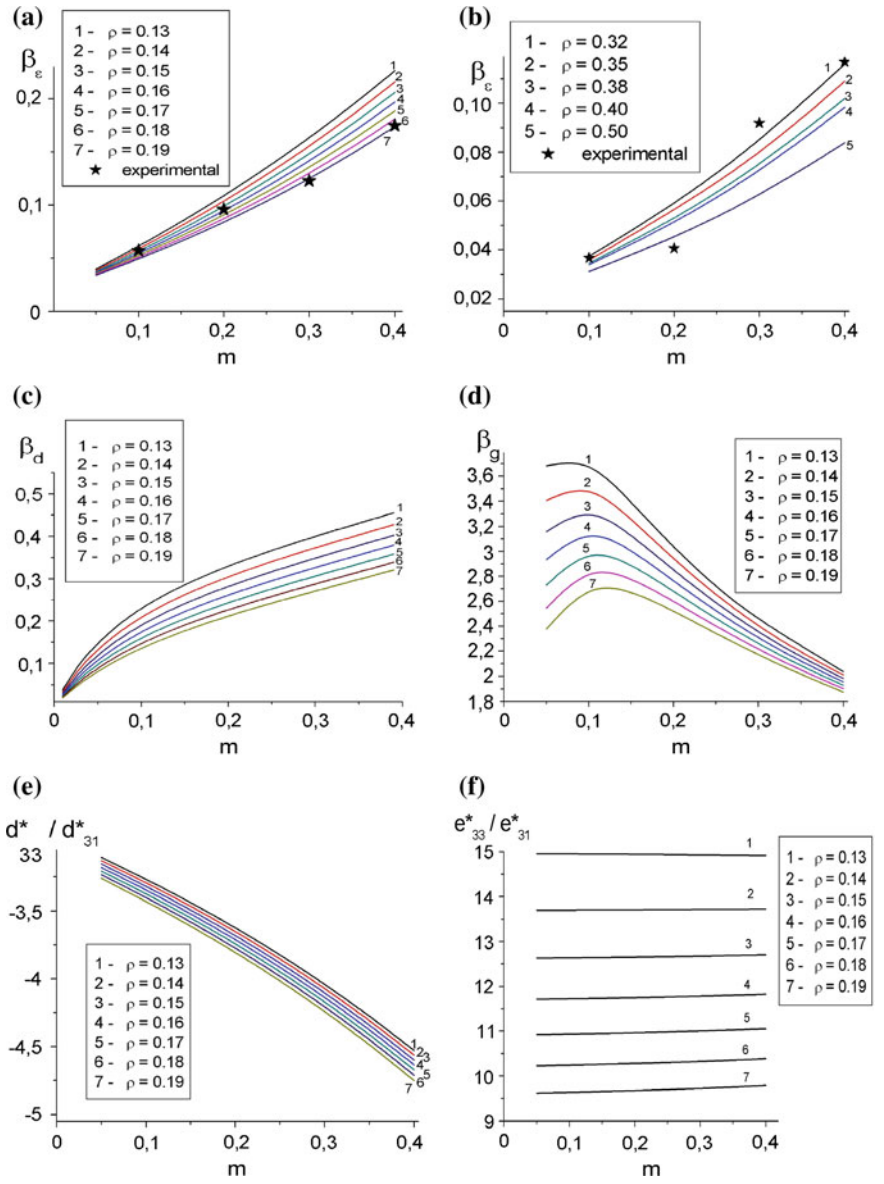

Fig. 5.2 Volume-fraction dependence of normalised dielectric permittivity β_ε (**a**), (**b**) normalised piezoelectric coefficients β_d (**c**) and β_d (**d**), and factors of the piezoelectric anisotropy ζ_d^* (**e**) and ζ_e^* (**f**) of the 0–3 $PbTiO_3$-based FC/epoxy composite. Graphs **a** and **b** correspond to the structured composite and unstructured composite, respectively. Experimental points are from dielectric measurements [12] (reprinted from paper by Topolov and Krivoruchko [22], with permission from Nova Science Publishers)

Table 5.1 Room-temperature values of elastic moduli c_{pq}^{E} (in 10^{10} Pa),[a] piezoelectric coefficients e_{fp} (in C / m^2) and dielectric permittivities ε_{ff}^{ξ} of FCs of the $PbTiO_3$ and PZT types

	$(Pb_{0.9625}La_{0.025})\cdot(Ti_{0.99}Mn_{0.01})O_3$ (modified $PbTiO_3$)[b] [21]	$(Pb_{0.80}Ca_{0.20})\cdot TiO_3^c$ [19]	$(Pb_{0.75}Ca_{0.25})\cdot TiO_3^c$ [19]	ZTS-19 [13][b]
c_{11}^{E}	14.33	18.5	18.9	10.9
c_{12}^{E}	3.220	4.76	5.19	6.1
c_{13}^{E}	2.413	4.68	5.06	5.4
c_{33}^{E}	13.16	18.0	18.3	9.3
c_{44}^{E}	5.587	6.79	6.76	2.4
e_{31}	0.4584	0.844	1.33	–4.9
e_{33}	6.499	4.31	5.09	14.9
e_{15}	5.923	1.77	1.95	10.6
$\varepsilon_{11}^{\xi}/\varepsilon_0$	210	126	152	820
$\varepsilon_{33}^{\xi}/\varepsilon_0$	140	123	147	840

[a] FCs poled along the OX_3 axis are characterised [3, 13–15] by ∞mm symmetry and a relation $c_{66} = (c_{11}^{E} - c_{12}^{E})/2$

[b] Experimental values of the PZT-type FC

[c] Electromechanical constants have been calculated using the EMM. Spherical grains of the FC sample are assumed to be split into 90° lamellar domains of two types with equal volume fractions, and these domains are separated by planar 90° domain walls. These domain walls are assumed to be almost motionless so that a contribution from their displacements under external electric or mechanical fields into the electromechanical constants of the ceramic approaches zero [19]

components on the piezoelectric coefficients e_{3j}^{*} in the presence of the prolate FC inclusions (Fig. 5.1). Changes in the anisotropy factor ζ_d^{*} are observed in a narrow range, while the system of the isolated FC inclusions is surrounded by the piezo-passive polymer matrix, that impedes an electromechanical interaction between the inclusions. On increasing the volume fraction m, $|\zeta_d^{*}|$ increases (Fig. 5.2e) due to the large anisotropy factor $d_{33}^{(1)}/d_{31}^{(1)}$ of the modified $PbTiO_3$ FC, and in this case the aspect ratio ρ cannot strongly influence $\zeta_d^{*}(m)$.

5.1.2 Variations of the Anisotropy Factors

In Sect. 5.1.2 we discuss examples of changes in the anisotropy factors $\zeta_d^{*}(m)$ and $\zeta_k^{*}(m)$ in the 0–3 FC-based composites and choose FC compositions with different ratios $d_{33}^{(1)}/|d_{31}^{(1)}|$ and $e_{33}^{(1)}/e_{31}^{(1)}$. For example, the $(Pb_{1-x}Ca_x)O_3$ FC is characterised by ratios $d_{33}^{(1)}/|d_{31}^{(1)}| > 10$ and $e_{33}^{(1)}/e_{31}^{(1)} \approx 4$–5 at $e_{ij}^{(1)} > 0$ [19], while the ZTS-19 FC based on $Pb(Zr_{1-x}Ti_x)O_3$ is characterised by moderate ratios $d_{33}^{(1)}/|d_{31}^{(1)}|$ and $e_{33}^{(1)}/|e_{31}^{(1)}|$ [13] (see full sets of electromechanical constants in Table 5.1).

To compare results, we use two methods for averaging the electromechanical properties, namely, the EFM [see Eq. (4.22)] and FEM. The COMSOL package [23] is applied to obtain the volume-fraction dependence of the effective electromechanical properties of the 0–3 composite within the framework of the FEM. A representative unit cell, containing the spheroidal inclusion (Fig. 5.3a) with a radius adjusted to yield the appropriate volume fraction m, is discretised using tetrahedral elements [24]. Their number, depending on the aspect ratio ρ of the spheroidal inclusion, varies from 320,000 to 760,000. The unknown displacement and electric-potential fields are interpolated using linear Lagrangian shape functions. The corresponding number of degrees of freedom varies from 200,000 to 500,000. Periodic boundary conditions are enforced on the boundary of the representative unit cell. The matrix of effective constants of the composite is computed column-wise, performing calculations for diverse average strain and electric fields imposed to the structure. The Geometric Multigrid [25] iterative solver (V-cycle, successive over-relaxation pre- and post-smoother, direct coarse solver) is employed. After solving the electroelastic equilibrium problem, the effective electromechanical constants of the 0–3-composite are computed, by averaging the resulting local stress and electric-displacement fields over the unit cell shown in Fig. 5.3a. In both the EFM [3] and FEM [24] the matrix of the effective electromechanical properties $\| C^* \|$ is represented in the form (4.1) and regarded as a function of m and ρ.

Graphs in Fig. 5.3b–d suggest that the EFM and FEM data on the anisotropy factors from (4.24) are consistent for the $(Pb_{1-x}Ca_x)O_3$-based composite. Some discrepancies, especially at $m > 0.2$, are due to the electromechanical interaction between the FC inclusions being taken into account in the FEM averaging procedure. In the composite with the softer polymer matrix (data in Fig. 5.3d) differences between the curves calculated using the EFM and FEM become more pronounced. This means that the so-called effective field would have a stronger influence on the effective properties in the case of the stiffer matrix, however this peculiarity of the electromechanical interaction is not emphasised in the EFM averaging procedure and Eq. (4.22). Data from Fig. 5.3b–d are of interest for sensor and antenna applications of the composite while conditions $|\zeta_d^*| > 5$ and $|\zeta_k^*| > 5$ hold simultaneously.

The next example is concerned with the anisotropy factors $\zeta_d^*(m)$ and $\zeta_k^*(m)$ of a 0–3 ZTS-19 FC / clay composite with spheroidal inclusions. Clay is an isotropic material with Young modulus 300 MPa, Poisson's ratio 0.30 and dielectric permittivity 8.0 [26, 27]. The EFM prediction of the effective properties of the 0–3 composite was carried out using Eq. (4.22), and the FEM modelling was performed using the COMSOL package [23] as described above.

The anisotropy factor $\zeta_d^*(m)$ is represented by either an increasing or decreasing dependence, and some differences between values of $\zeta_k^*(m)$ calculated using the EFM and FEM are observed (Fig. 5.4). These discrepancies are accounted for by an approximate character of the EFM and by not taking into account the internal electroelastic fields when considering the FC component exhibiting considerable piezoelectric activity (for instance, in ZTS-19 $d_{3j}^{(1)} \sim 10^2$ pC / N [28]). A comparison of graphs in Fig. 5.4 enables us to conclude that the prolate shape of the spheroidal

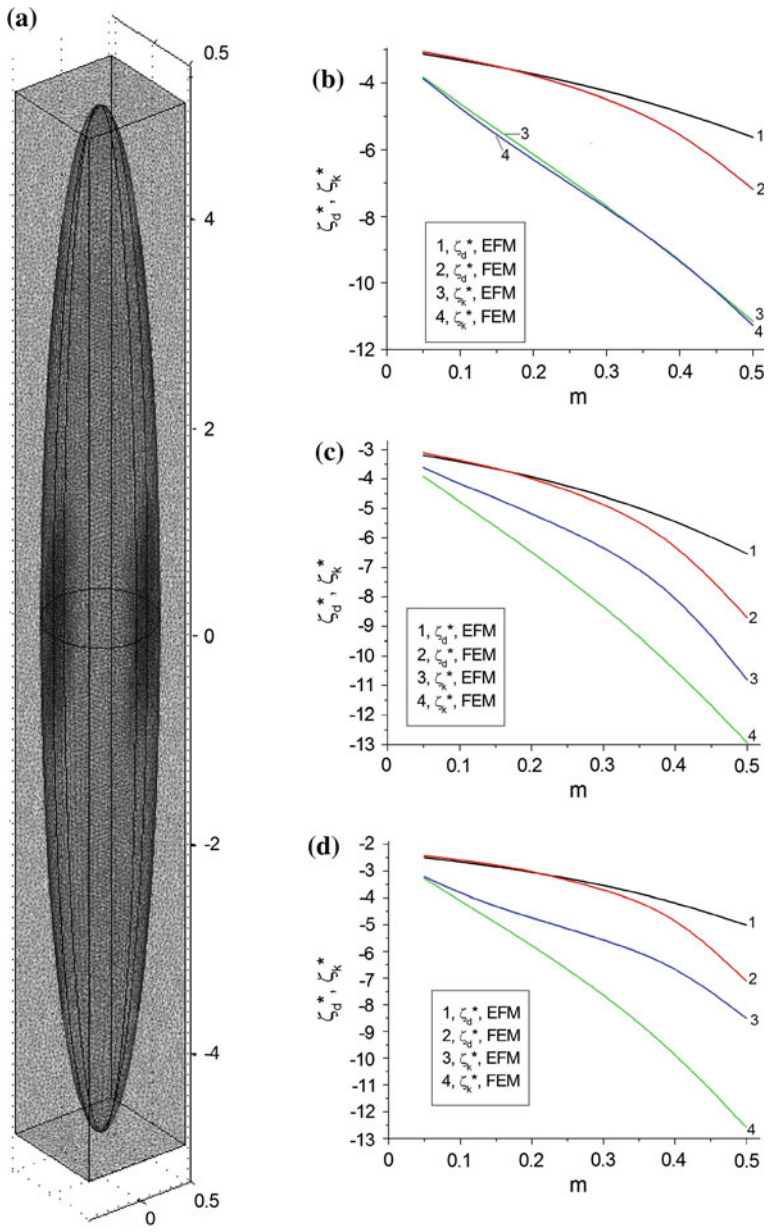

Fig. 5.3 Representative unit cell of the 0–3 composite (**a**) with spheroidal inclusions at FEM modelling and anisotropy factors ζ_d^* and ζ_k^* which have been calculated for the following 0–3 composites at $\rho = 0.1$: $(Pb_{0.80}Ca_{0.20})O_3$ FC/araldite (**b**) $(Pb_{0.75}Ca_{0.25})O_3$ FC/araldite (**c**) and $(Pb_{0.75}Ca_{0.25})O_3$ FC/elastomer (**d**)

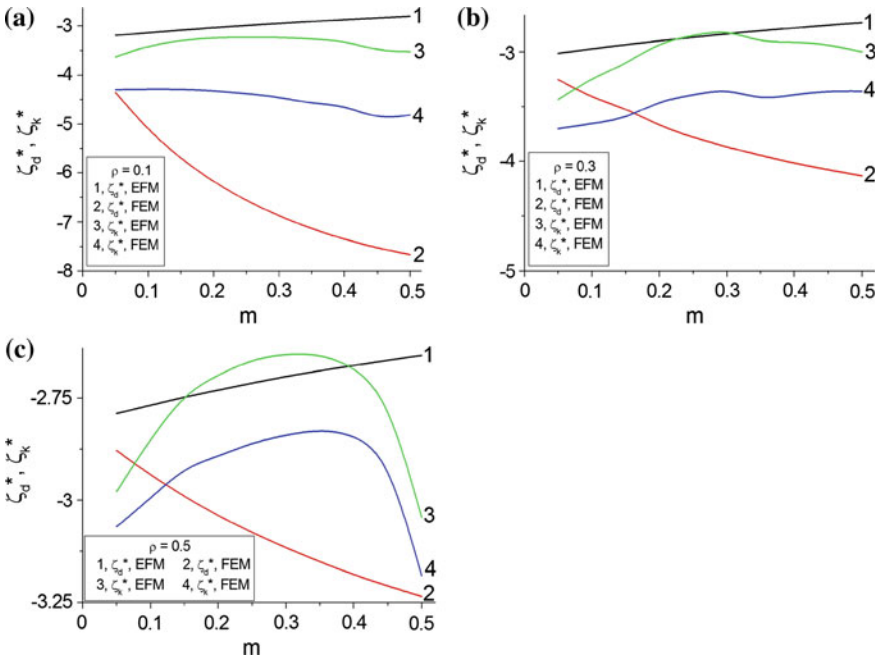

Fig. 5.4 Anisotropy factors ζ_d^* and ζ_k^* which have been calculated for the 0–3 ZTS-19 FC/clay composite with spheroidal inclusions at $\rho = 0.1$ (**a**), 0.3 (**b**), 0.5 (**c**)

inclusions (Fig. 5.1) in the composite sample promotes and increasing $|\zeta_d^*|$, but in a restricted range only. Variations of ζ_k^* are observed in the restricted ranges irrespective of the aspect ratio ρ (see curves 3 and 4 in Fig. 5.4). We remind the reader that ζ_d^* and ζ_k^* are linked in accordance with (4.24), and therefore, the elastic anisotropy of the studied composite does not promote a large increase of $|\zeta_k^*|$ with changes in m and ρ. It should be added that the piezoelectric activity of the ZTS-19 FC / clay composite rapidly decreases as the aspect ratio ρ increases at m = const.

Thus, the above-given examples show that high values of $|\zeta_d^*|$ and $|\zeta_k^*|$ can be simultaneously reached in $(Pb_{1-x}Ca_x)O_3$-based composites (Fig. 5.3b–d). This composite contains the highly anisotropic piezo-active component [$(Pb_{1-x}Ca_x)O_3$ FC, $x = 0.20$ or 0.25] distributed as a system of the aligned prolate spheroidal inclusions, and this circumstance plays the dominating role in forming the anisotropic 0–3 composite.

5.2 Relaxor-Ferroelectric Single Crystal/Polymer Composites

In Sect. 5.2 we consider examples of the performance of 0–3 composites with spheroidal SC inclusions (Fig. 5.1) that are uniformly aligned in the matrix and form a

periodic structure. It is assumed, that the main crystallographic axes x, y and z in each inclusion obey conditions x $\parallel OX_1$, y $\parallel OX_2$ and z $\parallel OX_3$, and centres of symmetry of the inclusions occupy sites of a simple lattice with unit-cell vectors parallel to the OX_j axes. The SC inclusions have a spontaneous polarisation $\boldsymbol{P}_s^{(1)} \parallel$ z $\parallel OX_3$, and the composite sample as a whole is poled along the OX_3 axis.

To determine the effective electromechanical properties of the 0–3 SC/polymer composite, we apply averaging procedures [3, 24] that allow for an electromechanical interaction between the piezo-active SC inclusions in the surrounding medium. This medium can be either piezo-passive or piezo-active, but the piezoelectric activity of the SC incluison remains higher than that of the surrounding medium. The first procedure is based on the EFM, the second procedure is based on the EMM, and the third procedure is concerned with the FEM modelling by means of the COMSOL package (details are in Sect. 5.1.2). In the EFM approach the full set of electromechanical constants of the composite is determined from (4.22). In the EMM approach a single inclusion is considered to be surrounded by a homogenised (effective) medium, and this medium is regarded as a matrix with the similar inclusions. The effective electromechanical properties of the 0–3 composite are found according to the EMM [3, 24] from the matrix

$$\parallel C^* \parallel = \parallel C^{(2)} \parallel + m(\parallel C^{(1)} \parallel - \parallel C^{(2)} \parallel) \parallel A \parallel . \tag{5.2}$$

The matrix $\parallel A \parallel$ from (5.2) is related to the boundary conditions in the "inclusion—surrounding medium" region (see Fig. 5.1) and represented [3, 19, 22, 24] as

$$\parallel A \parallel = [\parallel I \parallel + \parallel S \parallel \parallel C^* \parallel^{-1} (\parallel C^{(1)} \parallel - \parallel C^* \parallel)]^{-1}, \tag{5.3}$$

where $\parallel I \parallel$ is the 9×9 identity matrix, $\parallel S \parallel$ is the 9×9 matrix containing components of the Eshelby electroelastic tensor [20], and $\parallel C^* \parallel$ is the 9×9 matrix from (5.2). It should be noted that elements of $\parallel S \parallel$ from (5.3) depend on electromechanical constants of the matrix of the 0–3 composite and on the aspect ratio $\rho = a_1/a_3$ of the spheroidal inclusion (Fig. 5.1). In the EMM [24] the effective electromechanical properties of the composite (i.e., elements of $\parallel C^* \parallel = \parallel C^*(m, \rho) \parallel$) are evaluated as a result of a series of iterations involving (5.2) and (5.3). In the three aforementioned methods, i.e., within the framework of the EFM, EMM and FEM approaches, the effective properties of the composite are determined in the long-wave approximation [3]. This approximation is appropriate in a case when the wavelength of an external acoustic field is much longer than the semi-axes a_1 and a_3 of the separate inclusion (see Fig. 5.1).

5.2.1 Electromechanical Properties

To predict the performance of the 0–3 composite, we use full sets of experimental values of elastic moduli $c_{ab}^{(n),E}$, piezoelectric coefficients $e_{ij}^{(n)}$ and dielectric permittivities $\varepsilon_{pq}^{(n),\xi}$ [3, 19, 24]. These constants are involved in $\| C^{(n)} \|$ from (5.2) and (5.3). Among the relaxor-ferroelectric SC components, of particular interest is the PMN–0.33PT composition [29] chosen near the MPB. As is known, at room temperature the single-domain PMN–0.33PT SC is characterised by a rhombohedral distortion of the perovskite unit cell (3*m* symmetry, see Sect. 2.1). However, the domain-engineered PMN–0.33PT SC [29] poled along the perovskite unit-cell axis z ∥ [001] is characterised by macroscopic 4*mm* symmetry and four domain types (Fig. 2.4) that provide the effective spontaneous polarisation $\boldsymbol{P}_s^{(1)} \parallel OX_3$ of the SC sample. Electromechanical constants of the domain-engineered PMN–0.33PT SC are given in Table 5.2[1]. It should be added that this domain-engineered SC shows a high piezoelectric activity ($d_{3j}^{(1)} \sim 10^3$ pC / N) [29] and a considerable anisotropy of the piezoelectric coefficients $e_{3j}^{(1)}$: as follows from Table 5.2, $e_{33}^{(1)}/|e_{31}^{(1)}| = 5.6$.

Now we compare results on the effective properties and related parameters in a 0–3 PMN–0.33PT SC/araldite composite. In an attempt to attain large absolute values of the longitudinal piezoelectric coefficients $\Phi_{33}^*(\Phi = e, d, g,$ and $h)$ in the composite and to weaken the depolarising electric field therein in the presence of the SC inclusions, we consider a case of the prolate inclusions ($0 < \rho < 1$). Graphs in Fig. 5.4 suggest that the prolate shape of the SC inclusion with the lower ρ value leads to a higher composite piezoelectric activity at m = const. This prolate geometry also helps attain high piezoelectric sensitivity (i.e., large values of the piezoelectric coefficient $g_{33}^* = d_{33}^*/\varepsilon_{33}^{*\sigma}$) due to the large piezoelectric coefficient d_{33}^* combined [3] with a relatively low dielectric permittivity $\varepsilon_{33}^{*\sigma}$ of the studied composite at $0 < m < 0.1$.

The reason for the difference between the values of the piezoelectric coefficients Φ_{33}^* calculated using different methods (see Fig. 5.5a–d) is possibly due to the relatively small ratio of the elastic moduli of the PMN–0.33PT SC and araldite (see Table 5.2). At the same time we have large ratios of dielectric permittivities of the SC and polymer components. This may also explain the difference between values of dielectric permittivity $\varepsilon_{33}^{*\xi}$ (Fig. 5.5e). The matrix of effective constants $\| C^* \|$ from (4.22) and (5.2) contains the piezoelectric coefficients e_{ij}^*, elastic moduli c_{ab}^{*E} and dielectric permittivities $\varepsilon_{pp}^{*\xi}$, and these constants are calculated directly following the EFM, EMM or FEM. According to our evaluations involving the electromechanical constants of the PMN–0.33PT SC (component 1) and araldite (component 2), the ratios $c_{11}^{(1),E}/c_{11}^{(2)} = 14.7$ and $c_{33}^{(1),E}/c_{11}^{(2)} = 13.2$ are an order-of-magnitude less than $\varepsilon_{33}^{(1),\xi}/\varepsilon_{33}^{(2)} = 170$. This distinction leads to a significant re-distribution of internal

[1] Hereafter in Chap. 5 we use the notation "PMN–0.33PT SC" that is related to the domain-engineered SC sample with 4*mm* symmetry [29] and electromechanical constants listed in Table 5.2

electric and mechanical fields in the 0–3 PMN–0.33PT SC / araldite composite and enables us to believe that the EFM could be applied with some restrictions for 0–3 connectivity. We note that a similar mutual arrangement of curves $e^*_{33}(m)$ and $d^*_{33}(m)$ from EFM, FEM and EMM data [24] takes place in case of the 0–3 FC / polymer composite.

The ratios $c^{(1),E}_{11}/c^{(2)}_{11} \approx 19$, $c^{(1),E}_{33}/c^{(2)}_{11} \approx 16$ and $\varepsilon^{(1),\xi}_{33}/\varepsilon^{(2)}_{33} \approx 110$ hold, and an order-of-magnitude difference between dielectric constants is again attained. However, it should be added for comparison, that in work [35] on the 1–3 $PbTiO_3$-type FC/polymer composite with circular cylindrical inclusions (i.e., in case of $\rho = 0$), good agreement between the parameters calculated using both EFM and FEM is observed in a wide volume-fraction range. The 1–3 composite based on the $PbTiO_3$-type FC consists of components, for which ratios $c^{(1),E}_{11}/c^{(2)}_{11} \approx 24$, $c^{(1),E}_{33}/c^{(2)}_{11} \approx 23$ and $\varepsilon^{(1),\xi}_{33}/\varepsilon^{(2)}_{33} \approx 31 - 37$ [35] are true and no aforementioned order-of-magnitude difference is observed.

The striking difference between values of $\varepsilon^{*\sigma}_{33}$ evaluated at volume fractions $m > 0.2$ (see, for example, curves 1, 3 and 5 in Fig. 5.4f) is related to the difference between values of $\varepsilon^{*\xi}_{33}$ (Fig. 5.4e) and to the considerable piezoelectric effect in the composite with the PMN–0.33PT SC inclusions. On increasing the volume fraction of the SC, m, absolute values of the piezoelectric coefficients $|e^*_{3j}|$ and $|d^*_{3j}|$ increase

Table 5.2 Room-temperature values of elastic moduli c^E_{pq} (in 10^{10} Pa), piezoelectric coefficients e_{fp} (in C/m^2) and dielectric permittivities ε^{ξ}_{ff} of some components of composites

	PMN–0.33PT SC[a] [29]	$(Pb_{0.76}Ca_{0.24})TiO_3$ SC[b] [30]	PMN–0.35PT FC[c] [31]	VDF–TrFE[d] [32]	Araldite[e] [33]
c^E_{11}	11.5	26.6	14.67	0.85	0.78
c^E_{12}	10.3	15.1	8.84	0.36	0.44
c^E_{13}	10.2	9.42	9.68	0.36	0.44
c^E_{33}	10.3	7.53	14.78	0.98	0.78
c^E_{44}	6.9	7.81	2.99	–	0.17
c^E_{66}	6.6	13.2	2.92	0.25	0.17
e_{31}	–3.9	0.653	–5.0	0.007	0
e_{33}	20.3	6.48	28.0	–0.222	0
e_{15}	10.1	5.36	14.3	–	0
$\varepsilon^{\xi}_{11}/\varepsilon_0$	1,434	171	1,650	–	4.0
$\varepsilon^{\xi}_{33}/\varepsilon_0$	680	66.4	2,650	6.0	4.0

[a] Domain-engineered SC, $4mm$ symmetry, experimental data
[b] Single-domain SC, $4mm$ symmetry, calculated data
[c] Poled textured FC, ∞mm symmetry, experimental data
[d] Elastic moduli c^E_{pq} and piezoelectric coefficients e_{fp} of 75 / 25 mol.% copolymer of vinylidene fluoride and trifluoroethylene (VDF–TrFE, ∞mm symmetry) were calculated using experimental values of elastic compliances s^E_{ab} and piezoelectric coefficients d_{ij} from work [32]. In our calculations, equalities $c^E_{44} \approx c^E_{66}$, $\varepsilon^{\xi}_{11} \approx \varepsilon^{\xi}_{33}$ and $e_{15} \approx -e_{33}$ are assumed [34] to be correct for VDF–TrFE
[e] Piezo-passive polymer, experimental data

monotonically (see, for example Fig. 5.4a, b) and, therefore, the difference $\varepsilon_{33}^{*\sigma} - \varepsilon_{33}^{*\xi}$ caused by the piezoelectric effect [see Eq. (1.16)] increases.

The difference between values of k_{33}^* calculated using different methods (Fig. 5.5g) is primarily due to values of $\varepsilon_{33}^{*\sigma}$ (Fig. 5.5f) and d_{33}^* (Fig. 5.5b), which have also been calculated using different methods. Of specific interest are curves of $g_{33}^*(m)$ shown in Fig. 5.5c. The volume-fraction dependence of the piezoelectric coefficient $g_{33}^*(m) = d_{33}^*(m)/\varepsilon_{33}^{*\sigma}(m)$ is non-monotonic and is due to the combination of the piezoelectric $[d_{33}^*(m)]$ and dielectric $[\varepsilon_{33}^{*\sigma}(m)]$ properties, see graphs in Fig. 5.5b, f. The location of $\max g_{33}^*(m)$ strongly depends on the aspect ratio ρ of the inclusions: at $\rho = 0.1$, when the highly prolate SC inclusions in the polymer matrix give rise to a slight depolarising effect, $\max g_{33}^*(m)$ is found at small volume fractions $(0 < m < 0.05)$, and on increasing ρ, when the depolarising effect becomes stronger and dielectric permittivity $\varepsilon_{33}^{*\sigma}(m)$ increases slower, $\max g_{33}^*(m)$ shifts towards the larger values of m. A significant piezoelectric sensitivity for the composite ($g_{33}^* > 200$ mV· m / N, i.e., about 6 times more than $g_{33}^{(1)}$ of PMN–0.33PT SC [29]) is predicted in the presence of inclusions with $\rho = 0.1$ at volume fractions $m \leq 0.1$ (Fig. 5.5c).

5.2.2 *Role of the Longitudinal Piezoelectric Effect*

The PMN–0.33PT-based composite is also of interest due to the leading role of the longitudinal piezoelectric effect in forming the interconnections between the elastic, piezoelectric and dielectric properties [see formulae (1.12–1.19)]. The presence of the highly piezo-active prolate SC inclusions, irrespective of the piezoelectric properties of the matrix surrounding them, enables one to simplify links between the piezoelectric coefficients from (1.12–1.15) and interconnections between effective constants in (1.16–1.19) with taking into account symmetry of the composite. To show the role of the longitudinal piezoelectric coefficients Φ_{33}^*, we introduce ratios

$$R_1 = d_{33}^* e_{33}^* / (\varepsilon_{33}^{*\sigma} - \varepsilon_{33}^{*\xi}),\ R_2 = e_{33}^* s_{33}^{*E} / d_{33}^*,\ R_3 = h_{33}^* s_{33}^{*D} / g_{33}^*, \text{ and}$$
$$R_4 = k_t^* / k_{33}^* \tag{5.4}$$

and an anisotropy factor

$$\zeta_e^* = e_{33}^* / e_{31}^*. \tag{5.5}$$

Examples of the volume-fraction dependence of R_i and ζ_e^* from (5.4) and (5.5) are shown in Fig. 5.6. It should be mentioned that ratios R_i from (5.4) mainly comprise electromechanical constants that are determined indirectly while the matrix of the effective properties of the composite $\| C^* \|$ [see (4.22) and (5.2)] comprises e_{ij}^*, c_{ab}^{*E} and $\varepsilon_{pp}^{*\xi}$ only.

Due to $R_1 > 0.9$ (Fig. 5.6a), the piezoelectric contribution from the longitudinal piezoelectric effect (i.e., $d_{33}^* e_{33}^*$) into the difference between dielectric permittivities

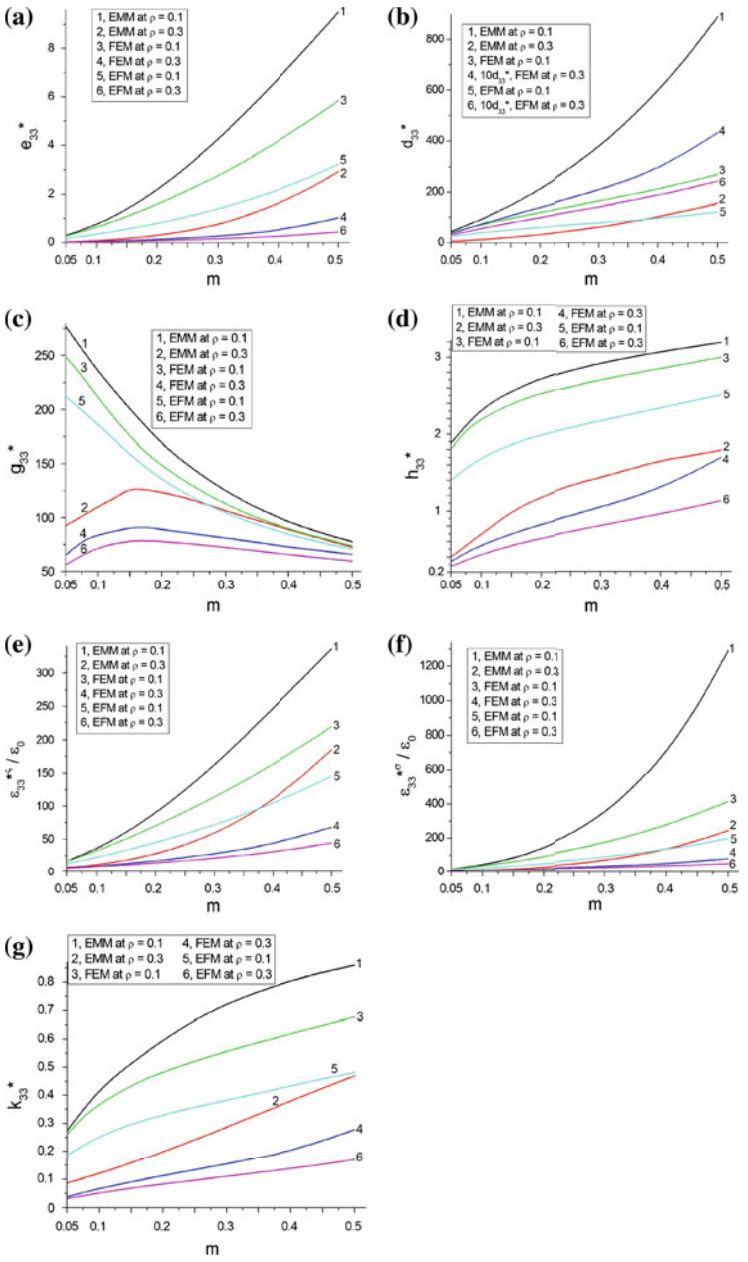

Fig. 5.5 Effective parameters calculated for the 0–3 PMN–0.33PT SC/araldite composite by means of the EMM, FEM and EFM: piezoelectric coefficients e^*_{33} (**a**, in C/m^2), d^*_{33} (**b**, in pC / N), g^*_{33} (**c**, in mV· m/N), and h^*_{33} (**d**, in GV/m), relative dielectric permittivities $\varepsilon^{*\xi}_{33}/\varepsilon_0$ (**e**) and $\varepsilon^{*\sigma}_{33}/\varepsilon_0$ (**f**), and ECF k^*_{33} (**g**) (reprinted from paper by Topolov et al. [24], with permission from Taylor and Francis)

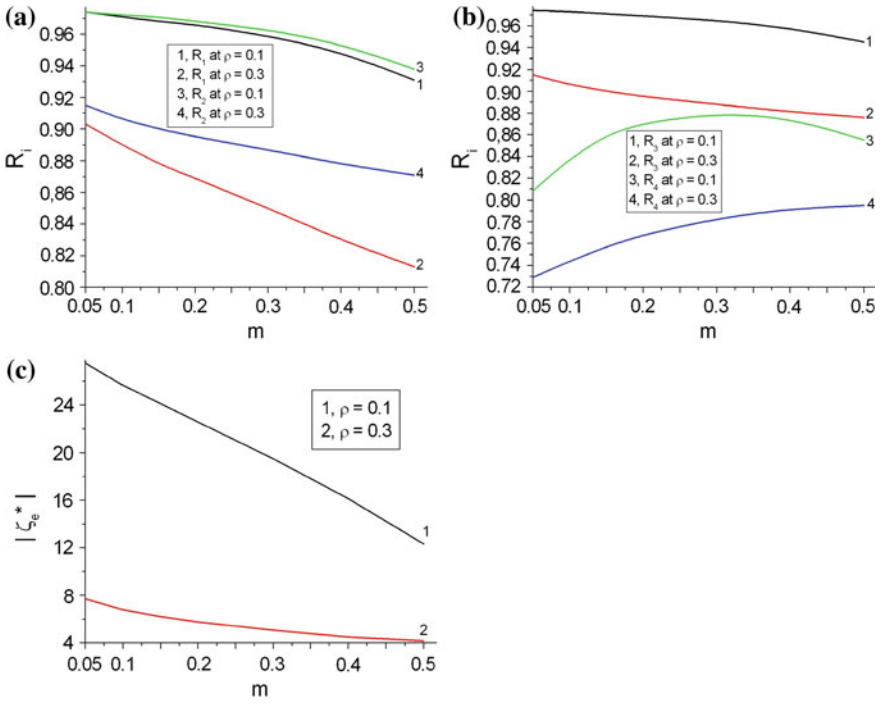

Fig. 5.6 Ratios R_i and anisotropy factor ζ_e^* which have been calculated for the 0–3 PMN–0.33PT SC/araldite composite by means of FEM

$\varepsilon_{33}^{*\sigma} - \varepsilon_{33}^{*\xi} = d_{33}^* e_{33}^* + 2d_{31}^* e_{31}^*$ [see (1.16)] can exceed 90 %. It is seen that at $\rho = 0.1$, the equality $R_1 = R_2$ holds with an accuracy to 1 % (cf. curves 1 and 3 in Fig. 5.6a), and the inequality $R_3 > R_1$ is valid in a wide volume-fraction range (Fig. 5.6a). As a result, the piezoelectric coefficient g_{33}^* that describes a longitudinal sensitivity of the composite has a negligible contribution from the transverse electromechanical interaction between the SC inclusion and the polymer matrix.

To understand the volume-fraction behaviour of R_4 at $\rho = \text{const}$ (see curves 3 and 4 in Fig. 5.6b), we remind the reader, that, in accordance with formulae [3, 36],

$$(k_t^*/k_{33}^*)^2 = [(e_{33}^*)^2/(c_{33}^{*D}\varepsilon_{33}^{*\xi})]/[(d_{33}^*)^2/(s_{33}^{*E}\varepsilon_{33}^{*\sigma})]. \tag{5.6}$$

Equation (5.6) can be simplified if to take into consideration equalities as follows: $c_{33}^{*D} = c_{33}^{*E}/[1 - (k_t^*)^2]$, $\varepsilon_{33}^{*\xi} = \varepsilon_{33}^{*\sigma}[1 - (k_t^*)^2]$ [36] and $d_{33}^* \approx e_{33}^* s_{33}^{*E}$ (that holds at $R_2 \approx 1$, see, for instance, Fig. 5.6a). Thus, the relation $R_4 \approx (c_{33}^{*E} s_{33}^{*E})^{-1/2}$ is valid. The largest values of $R_4 \approx 0.9$ (see curve 3 in Fig. 5.6b) and the equality

$$k_t^* \approx k_{33}^* \tag{5.7}$$

are achieved at $\rho = 0.1$. We note for comparison that relation (5.7) holds in the conventional 1–3 FC / polymer composite [32], and the aspect ratio $\rho = 0.1$ enables us to surmise that a distinction between the electromechanical properties of the studied 0–3 composite with prolate inclusions and the related 1–3 composite becomes minor.

As follows from Fig. 5.6c, $|\zeta_e^*(m)|$ decreases monotonically at ρ = const, and a similar monotonic decrease is also peculiar to $R_1(m)$ and $R_2(m)$ (see Fig. 5.6a). The reason for this correlation is the transverse piezoelectric response of the composite.

On increasing the volume fraction m the electromechanical interaction between the SC inclusions in the composite becomes more significant and therefore, the role of the piezoelectric coefficient $e_{31}^*(m)$ in forming the effective electromechanical properties increases.

5.2.3 *Effect of the Poling Direction on the Piezoelectric Properties and Their Anisotropy*

An important possibility is the ability to vary the electromechanical properties of the 0–3 composite using a change in the poling direction of the ferroelectric polymer component [9, 10]. A similar effect of the poling direction on the electromechanical properties was discussed in earlier studies [37] for 2–2 SC/polymer composites and may be important for piezo-technical applications. Below we show how the change in the poling direction of polymer influences the piezoelectric performance of the 0–3 composite based on PMN–0.33PT SC.

The effective electromechanical properties of the SC/polymer composite are determined within the framework of the model of the composite with spheroidal inclusions (Fig. 5.1) distributed regularly in a large matrix, and the FEM approach is used for our further calculations. The polymer matrix is characterised by a remanent polarisation vector that has one of the following directions: either $\boldsymbol{P}_r^{(2)} \uparrow\uparrow OX_3$ or $\boldsymbol{P}_r^{(2)} \uparrow\downarrow OX_3$. We remind that such modes of poling can be attained due to a large difference between coercive fields $E_c^{(n)}$ [38, 39] of the ferroelectric polymer and SC components. Among the ferroelectric polymer components of interest we choose VDF–TrFE (see electromechanical constants in Table 5.2) with $E_c^{(2)} \gg E_c^{(1)}$ at room temperature.

Data in Table 5.3 show the effect of the poling direction of the polymer component (i.e., the $\boldsymbol{P}_r^{(2)}$ orientation) on the piezoelectric coefficients and ECFs. To describe the anisotropy of these parameters, we use ζ_d^* and ζ_e^* from (4.24) and (5.1), respectively. Numerous changes in $\mathrm{sgn}d_{3j}^*$ and $\mathrm{sgn}e_{3j}^*$ take place in the presence of the polymer component with $\boldsymbol{P}_r^{(2)} \uparrow\uparrow OX_3$ (see Table 5.3). Such a poling direction of the polymer leads to the piezoelectric coefficients $d_{3j}^{(2)}$ and $e_{3j}^{(2)}$ whose signs differ from signs of $d_{3j}^{(1)}$ and $e_{3j}^{(1)}$ in PMN–0.33PT SC [29]. As a consequence, equations $d_{3j}^*(m) = 0$ and

Table 5.3 Piezoelectric coefficients d^*_{3j} (in pC / N) and e^*_{3j} (in C / m^2) and anisotropy factors ζ^*_d and ζ^*_e of the 0–3 PMN–0.33PT SC / VDF–TrFE composite (FEM caluclations)

ρ	m	d^*_{31}	d^*_{33}	$10^2 e^*_{31}$	e^*_{33}	ζ^*_d	ζ^*_e
	Polymer component with $\boldsymbol{P}_r^{(2)} \uparrow\uparrow OX_3$						
0.1	0.01	10.6	–34.0	0.488	–0.282	–3.21	–173
	0.03	9.17	–30.1	$-8.1 \cdot 10^{-3}$	–0.291	–3.28	$3.59 \cdot 10^3$
	0.05	8.19	–29.0	–0.471	–0.304	–3.54	64.5
	0.10	6.24	–25.8	–1.05	–0.333	–4.13	20.2
	0.20	2.87	–20.8	–4.63	–0.379	–7.25	7.54
	0.30	–0.070	–15.2	–9.30	–0.386	217	4.15
	0.40	–5.65	–6.19	–17.9	–0.270	1.10	1.51
	0.50	–16.8	–19.6	–38.0	0.499	11.7	–1.31
0.3	0.01	11.7	–37.7	0.521	–0.302	–3.22	–58.0
	0.03	11.0	–36.8	0.059	–0.322	–3.35	–546
	0.05	10.3	–35.8	–0.367	–0.339	–3.48	92.4
	0.10	8.67	–33.4	–1.45	–0.380	–3.85	26.2
	0.20	5.66	–29.5	–4.11	–0.457	–5.21	11.1
	0.30	2.71	–26.0	–8.13	–0.534	–9.59	6.57
	0.40	–0.80	–21.0	–15.0	–0.585	–26.3	3.90
	0.50	–7.57	–6.37	–30.4	–0.365	0.841	1.20
	Polymer component with $\boldsymbol{P}_r^{(2)} \uparrow\downarrow OX_3$						
0.1	0.01	–13.0	41.5	–0.780	0.332	–3.19	–42.6
	0.03	–13.5	43.4	–0.747	0.383	–3.21	–51.3
	0.05	–13.6	44.3	–0.719	0.423	–3.26	–58.8
	0.10	–13.7	45.7	–0.654	0.516	–3.34	–78.9
	0.20	–13.7	48.7	–0.536	0.719	–3.55	–134
	0.30	–14.5	53.9	–0.468	0.999	–3.72	–213
	0.40	–17.0	64.0	–0.624	1.46	–3.76	–234
	0.50	–25.1	90.9	–2.54	2.47	–3.62	–97.2
0.3	0.01	–12.3	39.5	–0.672	0.312	–3.21	–46.4
	0.03	–12.7	41.3	–0.501	0.349	–3.25	–69.7
	0.05	–12.9	42.4	–0.375	0.382	–3.29	–102
	0.10	–12.9	44.0	–0.124	0.458	–3.41	–369
	0.20	–12.6	46.1	0.338	0.615	–3.66	182
	0.30	–12.6	48.8	0.856	0.812	–3.87	94.9
	0.40	–13.1	53.2	1.36	1.10	–4.06	80.9
	0.50	–16.9	66.4	0.396	1.75	–3.93	442

$e^*_{3j}(m) = 0$ are achieved in a wide volume-fraction range and strongly influence the piezoelectric anisotropy of the 0–3 PMN–0.33PT SC / VDF–TrFE composite.

5.2.4 *Effect of the Arrangement of Inclusions on the Piezoelectric Properties and Their Anisotropy*

An additional effect needs to be considered when taking into account microgeometric features, i.e., a particular spatial distribution of the inclusions within the composite matrix. Poizat and Sester [40] analysed an effect of the arrangement of FC inclusions on the piezoelectric properties in 0–3 FC/polymer composites, however the similar effect was not considered in earlier studies on the SC/polymer composites, especially in the presence of relaxor-ferroelectric components with high piezoelectric activity. In Sect. 5.2.4 we consider 0–3 SC/polymer composites with a regular distribution of spheroidal inclusions in a matrix. In the first case the centres of symmetry of these inclusions occupy corners of a simple cubic lattice, and in the second case we assume that the same centres of symmetry form a body-centered cubic lattice. These distinctions in the arrangement influence both the longitudinal and transverse piezoelectric responses of the composite. It is assumed in both the cases that the spontaneous polarisation of each SC inclusion obeys a condition $\boldsymbol{P}_s^{(1)} \uparrow\uparrow OX_3$.

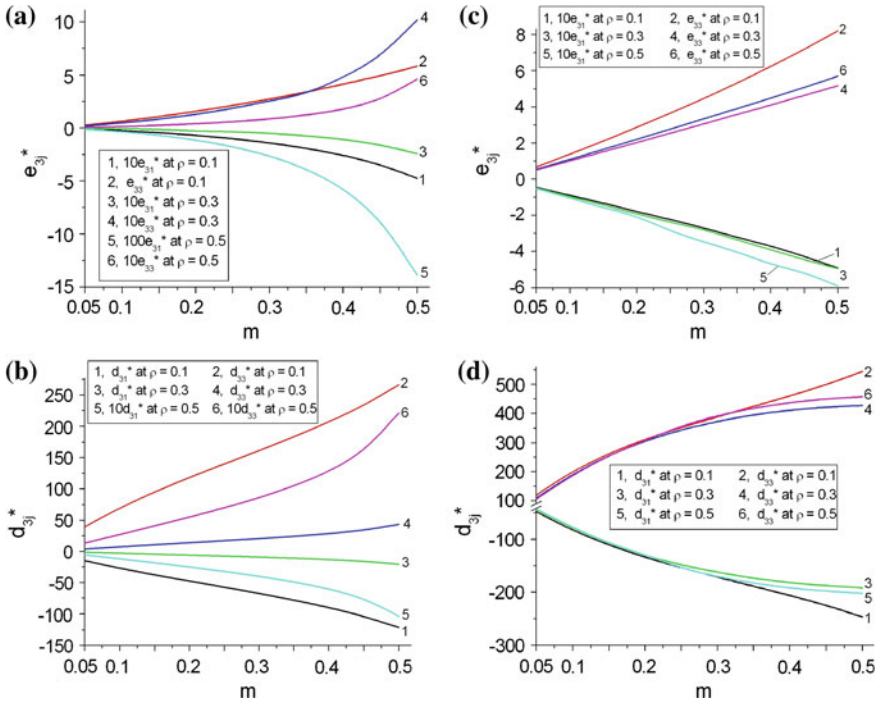

Fig. 5.7 Piezoelectric coefficients e_{3j}^* (**a** and **c**, in C/m^2) and d_{3j}^* (**b** and **d**, in pC/N) which have been calculated for the 0–3 PMN–0.33PT SC/araldite composite by means of FEM. Graphs a and b are related to the simple-cubic arrangement of the spheroidal SC inclusions in the polymer matrix, graphs c and d are related to the body-centered cubic arrangement of the spheroidal SC inclusions in the polymer matrix

Table 5.4 ECFs k^*_{3j}, k^*_t and k^*_p and anisotropy factos ζ^*_k and ζ^*_{t-p} of the 0–3 PMN–0.33PT SC/araldite composite (FEM calculations)

ρ	m	k^*_{33}	k^*_{31}	k^*_t	k^*_p	ζ^*_k	ζ^*_{t-p}
Composite with the simple-cubic arrangement of inclusions							
0.1	0.1	0.369	–0.112	0.370	–0.212	–3.29	–1.75
	0.3	0.559	–0.155	0.560	–0.308	–3.61	–1.82
	0.5	0.677	–0.206	0.680	–0.436	–3.29	–1.56
0.3	0.1	0.0664	–0.0244	0.0668	–0.0320	–2.72	–2.09
	0.3	0.153	–0.0505	0.156	–0.101	–3.03	–1.54
	0.5	0.278	–0.0836	0.287	–0.188	–3.33	–1.53
0.5	0.1	0.0275	–0.0113	0.0259	–0.0207	–2.43	–1.25
	0.3	0.0791	–0.0298	0.0823	–0.0589	–2.65	–1.40
	0.5	0.182	–0.0572	0.190	–0.129	–3.18	–1.47
Composite with the body-centered cubic arrangement of inclusions							
0.1	0.1	0.628	–0.232	0.629	–0.434	–2.71	–1.45
	0.3	0.756	–0.268	0.757	–0.533	–2.82	–1.42
	0.5	0.811	–0.291	0.812	–0.593	–2.79	–1.37
0.3	0.1	0.619	–0.248	0.621	–0.455	–2.50	–1.36
	0.3	0.749	–0.266	0.753	–0.512	–2.82	–1.47
	0.5	0.773	–0.289	0.778	–0.584	–2.67	–1.33
0.5	0.1	0.607	–0.247	0.609	–0.448	–2.46	–1.36
	0.3	0.748	–0.310	0.751	–0.589	–2.41	–1.28
	0.5	0.771	–0.309	0.773	–0.612	–2.50	–1.26

Examples of the volume-fraction dependence of the piezoelectric coefficients, ECFs and anisotropy factors, which are related to the aforementioned arrangements, are given in Fig. 5.7 and Table 5.4. To describe the anisotropy of ECFs (Table 5.4), we use two factors, ζ^*_k from (4.24) and

$$\zeta^*_{t-p} = k^*_t / k^*_p \tag{5.8}$$

where the thickness ECF k^*_t and the planar ECF k^*_p are given by (4.12).

The transition from the simple-cubic arrangement of inclusions to the body-centered cubic arrangement leads to an increase of $|e^*_{3j}|$, $|d^*_{3j}|$, $|k^*_{3j}|$, k^*_t, and k^*_p at fixed values of m and ρ. A more dense packing of the highly piezo-active inclusions in the 0–3 composite (i.e., the case of the body-centered cubic arrangement) leads to a more intensive electromechanical interaction between them even when they are embedded in the piezo-passive matrix. As a consequence, a higher piezoelectric performance is obtained (see Fig. 5.7c, d and Table 5.4) and a more pronounced transverse piezoelectric effect. The last circumstance gives rise to a decreasing $|\zeta^*_k|$ and $|\zeta^*_{t-p}|$ in a wide volume-fraction range. At the same time, the condition $|\zeta^*_e| \gg 1$ is valid (see, e.g., data in Fig. 5.7a, c), and the composite with a body-centered cubic arrangement of inclusions at $0.1 \leq \rho \leq 0.5$ remains similar to a 1–3 composite with the same components. An additional and essential argument for this analogy is that

the condition (5.7) related to 1–3 composites [32] is valid at various m and ρ values (see Table 5.4).

5.3 Single Crystal/Ceramic Composites

In the last decades, novel ferroelectric SC/FC ceramic composites have attracted the attention of researchers for several reasons. First, features of the synthesis and microstructure of such composites based on perovskite-type FCs have been studied [4, 5] to optimise the conditions for obtaining monolithic bulk samples with predictable properties. Second, in contrast to the well-known FC/polymer and SC/polymer composites, the SC/FC composite system contains components with comparable electromechanical properties. Third, there are restricted experimental data (see, for instance, work [5]) on the performance of the SC/FC composites that could be of importance for piezo-technical applications.

In Sect. 5.3 we discuss some examples of the electromechanical properties and anisotropy factors of the 0–3 SC / FC composites with spheroidal inclusions. Following the model of the 0–3 composite (Fig. 5.1), we regard component 1 as a SC and component 2 as a poled FC medium surrounding the SC inclusions. It is assumed that a body-centered cubic arrangement of the SC inclusions takes place therein, and the SC and FC components have the spontaneous polarisation vector $\boldsymbol{P}_s^{(1)} \uparrow\uparrow OX_3$ and the remanent polarisation vector $\boldsymbol{P}_r^{(2)} \uparrow\uparrow OX_3$, respectively. Hereafter we follow the FEM approach to calculate a full set of effective electromechanical constants and a series of effective parameters of the composite when varying the volume fraction m and aspect ratio ρ. The electromechanical constants of the components of the 0–3 composites to be considered are shown in Tables 5.1 and 5.2. Combining the properties of the components with equal or opposite signs of the piezoelectric coefficients $e_{3j}^{(n)}$ and with various anisotropy factors $e_{33}^{(n)}/e_{31}^{(n)}$, we obtain a series of important volume-fraction dependences of the effective piezoelectric properties, which are now discussed.

5.3.1 Two Components with a Large Anisotropy of Piezoelectric Coefficients $e_{3j}^{(n)} > 0$

We consider here a composite that consists of two components with related chemical compositions. Single-domain $(Pb_{0.76}Ca_{0.24})TiO_3$ SC and modified $PbTiO_3$ FC are characterised by a large anisotropy of the piezoelectric coefficients $e_{3j}^{(n)}$ and $\operatorname{sgn} e_{3j}^{(n)} > 0$ (see Tables 5.1, 5.2) and by moderate piezoelectric activity [21, 30]. Moreover, the anisotropy of the elastic moduli of the modified $PbTiO_3$ FC $c_{ab}^{(2),E}$ strongly differs from the elastic anisotropy of the conventional PZT-type FCs [3, 13, 28]. Such

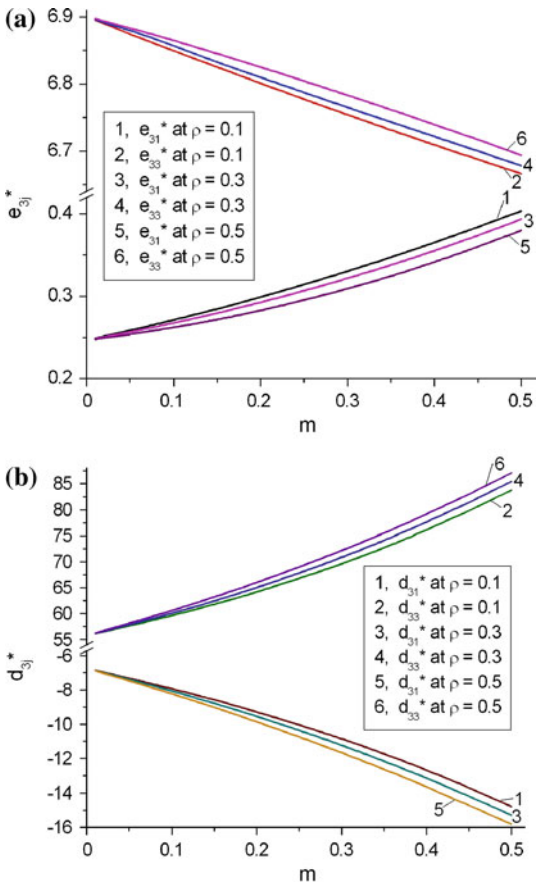

Fig. 5.8 Piezoelectric coefficients e^*_{3j} (**a**, in C/m^2) and d^*_{3j} (**b**, in pC/N) which have been calculated for the 0–3 $(Pb_{0.76}Ca_{0.24})TiO_3$ SC/modified $PbTiO_3$ FC composite by means of FEM

a combination of piezo-active components enables us to obtain a unique volume-fraction dependence in terms of the piezoelectric properties (Fig. 5.8) of the 0–3 SC/FC composite. These properties are characterised by the following features:

(i) inequalities $\zeta^*_e > 10$ and $5 < |\zeta^*_d| < 10$ hold in the wide volume-fraction range,

(ii) a combination of components leads to the conditions $\operatorname{sgn} e^*_{31} = \operatorname{sgn} e^*_{33} > 0$ and $\operatorname{sgn} d^*_{31} = -\operatorname{sgn} d^*_{33} < 0$, and these signs coincide with those of the piezoelectric coefficients of the interacting components, and

(iii) minor changes in the volume-fraction dependences $e^*_{3j}(m)$ and $d^*_{3j}(m)$ are observed at variations of the aspect ratio ρ of the prolate SC inclusion, i.e., the shape of the inclusion does not play a key role in forming the piezoelectric properties of the composite.

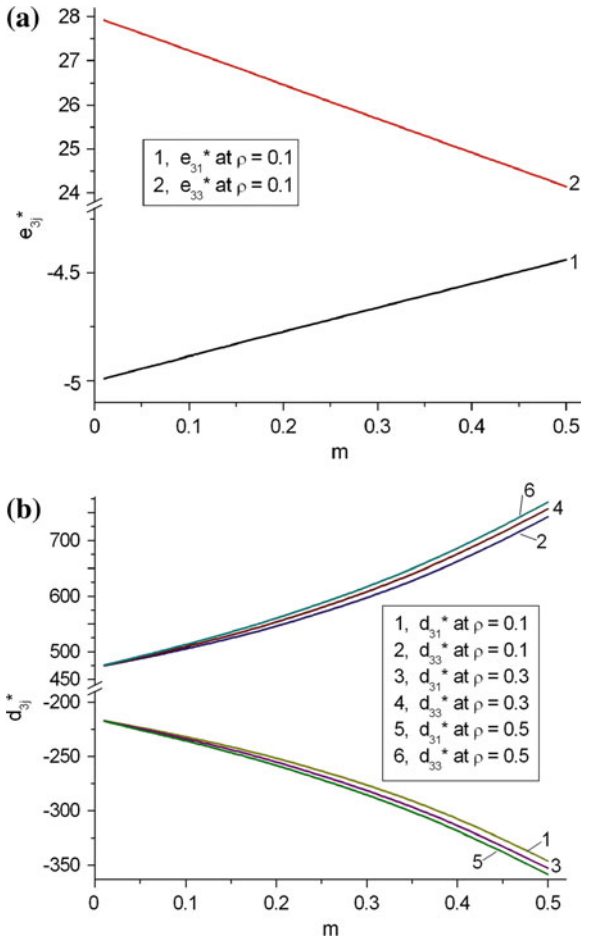

Fig. 5.9 Piezoelectric coefficients e^*_{3j} (**a**, in C/m^2) and d^*_{3j} (**b**, in pC/N) which have been calculated for the 0–3 PMN–0.33PT SC/PMN–0.35PT FC composite by means of FEM

5.3.2 Two Components with Piezoelectric Coefficients Obeying Conditions $sgn\, e_{33}^{(n)} = -sgn\, e_{31}^{(n)} > 0$

It is now assumed that the 0–3 composite consists of a system of PMN–0.33PT SC inclusions and a PMN–0.35PT FC matrix. The relative chemical compositions and high piezoelectric activity of the chosen SC and FC components along with the moderate ratios of the piezoelectric coefficients $d_{33}^{(n)}/d_{31}^{(n)}$ of the components [29, 31] predetermine the volume-fraction dependence of the effective properties in the composite. Examples of the piezoelectric properties of the studied SC / FC composite at variations of m and ρ are shown in Fig. 5.9.

Because of very minor changes in the volume-fraction dependence of $e^*_{3j}(m)$ at aspect ratios of ρ from 0.1 to 0.5, we have omitted the e^*_{3j} curves related to $0.1 < \rho \leq 0.5$ (see Fig. 5.9a). The reason for such behaviour of $e^*_{3j}(m)$ is due to the electromechanical interaction of the components with the piezoelectric coefficients $e^{(n)}_{3j}$ that obey a condition $e^{(1)}_{33}/e^{(1)}_{31} \approx e^{(2)}_{33}/e^{(2)}_{31}$. As an important consequence, a relation $\zeta^*_e \approx e^{(2)}_{33}/e^{(2)}_{31}$ is valid in a wide range of both m and ρ. The relatively minor changes in $d^*_{3j}(m)$ at $0.1 \leq \rho \leq 0.5$ (Fig. 5.9b) are mainly accounted for by a difference between the elastic anisotropy of the SC and FC components (compare data on elastic moduli c^E_{ab} in Tables 5.1 and 5.2). As in the case considered in Sect. 5.3.1, we state that the shape of the SC inclusion plays no major role in forming the piezoelectric properties of the composite studied.

5.3.3 *Components with Piezoelectric Coefficients Obeying Conditions* $\mathbf{sgn\, e^{(1)}_{33} = -sgn\, e^{(1)}_{31} > 0}$ *and* $\mathbf{sgn\, e^{(2)}_{33} = sgn\, e^{(2)}_{31} > 0}$

A combination of a highly piezo-active PMN–0.33PT SC [29] and a highly anisotropic FC of modified $PbTiO_3$ with moderate piezoelectric activity [21] provides us with a new example of the effective properties of 0–3 composites. The different signs of the piezoelectric coefficients $e^{(n)}_{31}$ for the SC and FC components (see Tables 5.1, 5.2) lead to validity of the condition $e^*_{31}(m) = 0$ and to very large values of $|\zeta^*_e|$ in a specific m range. At the same time, the anisotropy factor ζ^*_d affected by the piezoelectric properties of the SC and FC components with $\mathrm{sgn}d^{(n)}_{33} = -\mathrm{sgn}d^{(n)}_{31} > 0$ changes in a restricted range. Some results of FEM modelling of the piezoelectric response of the 0–3 composites are shown in Fig. 5.10. As in Sect. 5.2.4, for comparison we consider two versions of the arrangement of the SC inclusions in the FC matrix, namely, a simple-cubic and body-centered cubic arrangements.

The graphs in Fig. 5.10 suggest that the piezoelectric performance of the composite does not undergo large changes at the transition from a simple-cubic arrangement of the SC inclusions to a body-centered cubic arrangement. It is seen that $e^*_{3j}(m)$ (Fig. 5.10a, c) and $d^*_{3j}(m)$ (Fig. 5.10b, d) vary in ranges that are weakly dependent on the aspect ratio ρ and features of the arrangement of the inclusions. The difference between the curves becomes negligible (see Fig. 5.10c, d) at the body-centered cubic arrangement, i.e., at the denser packing of the inclusions in the composite sample.

The relatively small values of $|\zeta^*_d|$ of the composite (in comparison to $d^{(2)}_{33}/|d^{(2)}_{31}| \approx 11.6$ in the $PbTiO_3$-type FC component [21]) over a wide m range implies that the highly piezo-active SC component plays a key role in forming the piezoelectric properties for this 0–3 SC/FC composite. It should be added that a similar situation, however with other values of $|\zeta^*_d|$, has been observed in ferroelectric SC/polymer

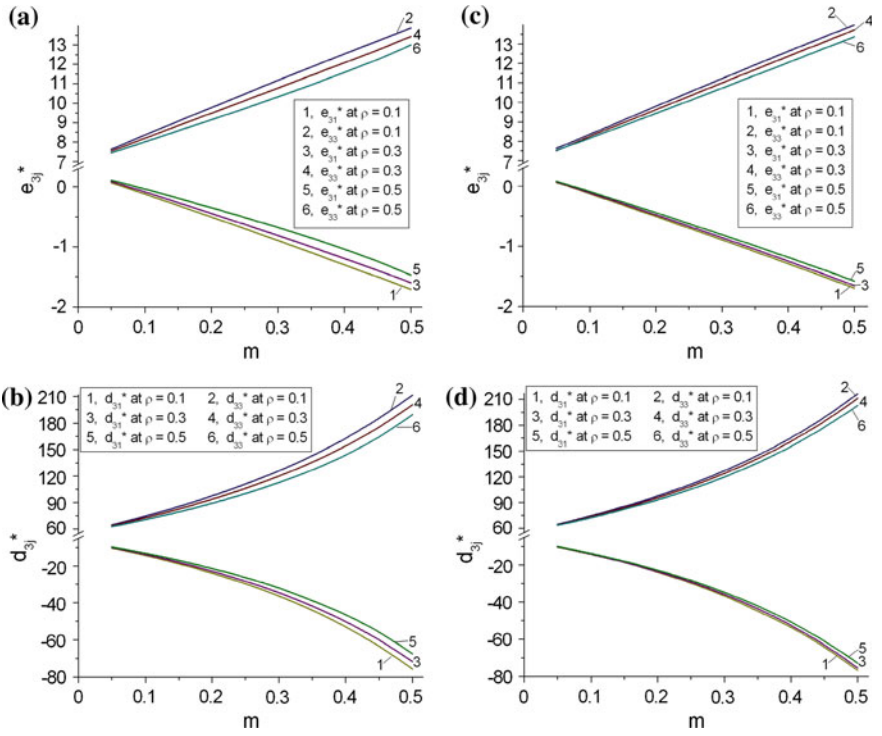

Fig. 5.10 Piezoelectric coefficients e^*_{3j} (**a** and **c**, in C / m^2) and d^*_{3j} (**b** and **d**, in pC / N) which have been calculated for the 0–3 PMN–0.33PT SC/modified $PbTiO_3$ FC composite by means of FEM. Graphs a and b are related to the simple-cubic arrangement of the spheroidal SC inclusions in the FC matrix, graphs c and d are related to the body-centered cubic arrangement of the spheroidal SC inclusions in the FC matrix

and FC / polymer composites (see Sects. 5.1 and 5.2). The key role of the SC component is also shown in Table 5.5: minor differences between the similar ECFs, related to the simple-cubic and body-centered cubic arrangement of the prolate inclusions, are achieved in a wide volume-fraction range. Otherwise, the FC matrix could not strongly affect the volume-fraction dependence of ECFs and anisotropy factors, and values of $|\zeta^*_k|$ and $|\zeta^*_{t-p}|$ rapidly decrease on increasing m at any type of the SC-inclusion arrangement. It is seen that the inequality $|\zeta^*_k| > 5$ holds at $m < 0.15$, i.e., at small volume fractions of the highly piezo-active SC component. Moreover, Eq. (5.7) holds in almost the whole volume-fraction range (see Table 5.5), and this circumstance resembles the relation between ECFs in the conventional 1–3 FC/polymer composite [32].

Table 5.5 ECFs k^*_{3j}, k^*_t and k^*_p and anisotropy factors ζ^*_k and ζ^*_{t-p} of the 0–3 PMN–0.33PT SC/modified $PbTiO_3$ FC composite at $\rho = 0.1$ (FEM calculations)

m	k^*_{33}	k^*_{31}	k^*_t	k^*_p	ζ^*_k	ζ^*_{t-p}
Composite with the simple-cubic arrangement of inclusions						
0.05	0.470	–0.0795	0.493	–0.131	–5.91	–3.76
0.10	0.511	–0.0988	0.512	–0.165	–5.17	–3.10
0.15	0.531	–0.118	0.531	–0.200	–4.50	–2.66
0.20	0.550	–0.136	0.551	–0.243	–4.04	–2.27
0.25	0.571	–0.154	0.572	–0.271	–3.71	–2.11
0.30	0.592	–0.171	0.593	–0.307	–3.46	–1.93
0.35	0.613	–0.189	0.615	–0.343	–3.24	–1.79
0.40	0.635	–0.207	0.637	–0.381	–3.07	–1.67
0.45	0.657	–0.225	0,660	–0.420	–2.92	–1.57
0.50	0.680	–0.243	0.683	–0.443	–2.80	–1.54
Composite with the body-centered cubic arrangement of inclusions						
0.05	0.492	–0.0799	0.492	–0.131	–6.16	–3.76
0.10	0.511	–0.0992	0.511	–0.166	–5.15	–3.08
0.15	0.530	–0.118	0.630	–0.200	–4.49	–3.15
0.20	0.550	–0.135	0.551	–0.235	–4.07	–2.34
0.25	0.571	–0.153	0.574	–0.271	–3.73	–2.12
0.30	0.593	–0.169	0.595	–0.307	–3.51	–1.94
0.35	0.615	–0.186	0.617	–0.344	–3.31	–1.78
0.40	0.638	–0.202	0.640	–0.382	–3.16	–1.68
0.45	0.661	–0.219	0.664	–0.421	–3.02	–1.58
0.50	0.685	–0.235	0.688	–0.462	–2.91	–1.49

5.4 Conclusion

Chapter 5 has been devoted to the piezoelectric performance and anisotropy of various matrix composites with 0–3 connectivity. Our modelling and property predictions have been carried out within the framework of the model of a 0–3 piezo-active composite with spheroidal inclusions distributed regularly in a large matrix (see a fragment in Fig. 5.1). The model concepts and methods for averaging the electromechanical properties (EMM, EFM and FEM) have been applied to 0–3 composites based on either FE or relaxor-ferroelectric SCs. The following combinations of components have been analysed in the context of the effective properties:

(i) $PbTiO_3$-type FC with a large ratio $d^{(1)}_{33}/|d^{(1)}_{31}|$/piezo-passive polymer,
(ii) PZT-type FC with a moderate ratio $d^{(1)}_{33}/|d^{(1)}_{31}|$/clay (piezo-passive component),
(iii) relaxor-ferroelectric SC with high piezoelectric activity/piezo-passive polymer,
(iv) relaxor-ferroelectric SC with high piezoelectric activity/piezo-active polymer,
(v) relaxor-ferroelectric SC with high piezoelectric activity/$PbTiO_3$-type FC with a large ratio $d^{(2)}_{33}/|d^{(2)}_{31}|$,

(vi) relaxor-ferroelectric SC with high piezoelectric activity/PZT-type FC with a moderate ratio $d_{33}^{(2)}/|d_{31}^{(2)}|$, and

(vii) ferroelectric SC with a large ratio $e_{33}^{(1)}/|e_{31}^{(1)}|$/$PbTiO_3$-type FC with a large ratio $d_{33}^{(2)}/|d_{31}^{(2)}|$.

For the combinations (i)–(vii) examples of the volume-fraction dependence of the piezoelectric coefficients, ECFs and anisotropy factors have been considered under the condition that the composite contains prolate spheroidal inclusions with a fixed aspect ratio ρ from a range $0.1 \leq \rho \leq 0.5$. Orientation effects caused by the poling direction of the ferroelectric polymer matrix and the arrangement of the SC inclusions in the polymer (or FC) matrix have been considered, and the role of these effects in forming the piezoelectric properties and their anisotropy in the 0–3 composites has been analysed. Examples of behaviour of ECFs and their anisotropy at different arrangements of the SC inclusions in the matrix (Tables 5.4, 5.5) have been discussed. It has been shown that the highly piezo-active SC inclusion influences the electromechanical properties and ECFs of the composite in different ways, depending on the piezoelectric properties and their anisotropy in the matrix of the 0–3 composite.

The four ratios (5.4) describing the interconnections between the effective electromechanical properties in 0–3 composites have been introduced to interpret features of the longitudinal dielectric and piezoelectric response of composite structures with prolate SC inclusions that exhibit high piezoelectric activity. Hereby the important role of piezoelectric anisotropy and activity of the composite components in the longitudinal piezoelectric effect has been analysed for 0–3 composites with a variety of combinations of components [see items (i)–(vii)].

Results of the study on the piezoelectric performance, anisotropy and orientation effects can be of value for piezo-technical, acoustic and other applications of modern piezo-active 0–3 composites as materials whose piezoelectric properties and anisotropy factors vary in wide ranges.

References

1. Akdogan EK, Allahverdi M, Safari A (2005) Piezoelectric composites for sensor and actuator applications. IEEE Trans Ultrason Ferroelectr Freq Control 52:746–775
2. Safari A, Akdogan EK (2006) Rapid prototyping of novel piezoelectric composites. Ferroelectrics 331:153–179
3. Topolov VYu, Bowen CR (2009) Electromechanical properties in composites based on ferroelectrics. Springer, London
4. Smotrakov VG, Eremkin VV, Alyoshin VA, Tsikhotsky ES (2000) Preparation and study of single-crystal-ceramic composite. Izv Akad Nauk Ser Fiz 64:1220–1223 (in Russian)
5. Takahashi H, Tukamoto S, Qiu J, Tani J, Sukigara T (2003) Property of composite ceramics composed of single crystals and ceramic matrix using hybrid sintering. Jpn J Appl Phys Pt 1(42):6055–6058
6. Chan HLW, Cheung MC, Choy CL (1999) Study on $BaTiO_3$/ P(VDF-TrFE) 0–3 composites. Ferroelectrics 224:113–120

7. Lam KH, Chan HLW, Luo HS, Yin QR, Yin ZW, Choy CL (2003) Dielectric properties of 65PMN-35PT / P(VDF-TrFE) 0–3 composites. Microelectron Eng 66:792–797
8. Ngoma JB, Cavaille JY, Paletto J (1990) Dielectric and piezoelectric properties of copolymer-ferroelectric composite. Ferroelectrics 109:205–210
9. Chan HLW, Ng PKL, Choy CL (1999) Effect of poling procedure on the properties of lead zirconate titanate / vinylidene fluoride-trifluoroethylene composites. Appl Phys Lett 74:3029–3031
10. Ng KL, Chan HLW, Choy CL (2000) Piezoelectric and pyroelectric properties of PZT/P(VDF-TrFE) composites with constituent phases poled in parallel or antiparallel directions. IEEE Trans Ultrason Ferroelectr Freq Control 47:1308–1315
11. Fang D-N, Soh AK, Li C-Q, Jiang B (2001) Nonlinear behavior of 0–3 type ferroelectric composites with polymer matrices. J Mater Sci 36:5281–5288
12. Wilson SA, Maistros GM, Whatmore RW (2005) Structure modification of 0–3 piezoelectric ceramic / polymer composites through dielectrophoresis. J Phys D: Appl Phys 38:175–182
13. Khoroshun LP, Maslov BP, Leshchenko PV (1989) Prediction of effective properties of piezo-active composite materials. Naukova Dumka, Kiev (in Russian)
14. Luchaninov AG (2002) Piezoelectric effect in non-polar heterogeneous ferroelectric materials. Volgograd State Academy of Architecture and Construction, Volgograd (in Russian)
15. Sokolkin YuV, Pan'kov AA (2003) Electroelasticity of piezo-composites with irregular structures. Fizmatlit, Moscow (in Russian)
16. Poon YM, Ho CH, Wong YW, Shin FG (2007) Theoretical predictions on the effective piezoelectric coefficients of 0–3 PZT / polymer composites. J Mater Sci 42:6011–6017
17. Levin VM, Rakovskaja MI, Kreher WS (1999) The effective thermoelectroelastic properties of microinhomogeneous materials. Int J Solids Struct 36:2683–2705
18. Levassort F, Topolov VYu, Lethiecq M (2000) A comparative study of different methods of evaluating effective electromechanical properties of 0–3 and 1–3 ceramic / polymer composites. J Phys D: Appl Phys 33:2064–2068
19. Glushanin SV, Topolov VYu, Krivoruchko AV (2006) Features of piezoelectric properties of 0–3-type ceramic / polymer composites. Mater Chem Phys 97:357–364
20. Huang JH, Yu S (1994) Electroelastic Eshelby tensors for an ellipsoidal piezoelectric inclusion. Compos Eng 4:1169–1182
21. Ikegami S, Ueda I, Nagata T (1971) Electromechanical properties of $PbTiO_3$ ceramics containing La and Mn. J Acoust Soc Am 50:1060–1066
22. Topolov VYu, Krivoruchko AV (2010) Ferroelectric $PbTiO_3$: from a single-domain state to composite components. In: Borowski M (ed) Perovskites: Structure, properties and uses. Nova Science Publishers, Hauppage, pp 481–499
23. COMSOL, Inc. COMSOLMultiphysics^{TM} user's guide (version 3.5a, 2008), http://www.comsol.com
24. Topolov VYu, Bisegna P, Bowen CR (2011) Analysis of the piezoelectric performance of modern 0–3-type composites based on relaxor-ferroelectric single crystals. Ferroelectrics 413:176–191
25. Hacksbusch W (1985) Multi-grid methods and applications. Springer, Berlin
26. Bowles JE (1996) Foundation analysis and design. McGraw-Hill, New York
27. Balkevich VL (1984) Technical ceramics. Stroyizdat, Moscow
28. Gorish AV, Dudkevich VP, Kupriyanov MF, Panich AE, Turik AV (1999) Piezoelectric device-making. Physics of ferroelectric ceramics, vol. 1. Radiotekhnika, Moscow (in Russian)
29. Zhang R, Jiang B, Cao W (2001) Elastic, piezoelectric, and dielectric properties of multidomain $0.67Pb(Mg_{1/3}Nb_{2/3})O_3$- $0.33PbTiO_3$ single crystals. J Appl Phys 90:3471–3475
30. Topolov VYu, Glushanin SV (2002) Effective electromechanical properties of ferroelectric piezoactive composites of the crystal-ceramic type based on $(Pb_{1-x}Ca_x)TiO_3$. Tech Phys Lett 28:279–282
31. Levassort F, Thi MP, Hemery H, Marechal P, Tran-Huu-Hue L-P, Lethiecq M (2006) Piezoelectric textured ceramics: effective properties and application to ultrasonic transducers. Ultrasonics 44:621–626

32. Taunaumang H, Guy IL, Chan HLW (1994) Electromechanical properties of 1–3 piezoelectric ceramic / piezoelectric polymer composites. J Appl Phys 76:484–489
33. Levassort F, Lethiecq M, Millar C, Pourcelot L (1998) Modeling of highly loaded 0–3 piezoelectric composites using a matrix method. IEEE Trans Ultrason Ferroelectr Freq Control 45:1497–1505
34. Topolov VYu, Glushanin SV, Panich AE (2004) Features of the piezoelectric response for a novel four-component composite structure. Ferroelectrics 308:53–65
35. Topolov VYu, Krivoruchko AV, Bisegna P (2008) Features of electromechanical properties of 1–3 composites based on $PbTiO_3$-type ceramics. J Phys D: Appl Phys 41:035406–035408
36. Ikeda T (1990) Fundamentals of piezoelectricity. Oxford University Press, Oxford, New York, Toronto
37. Topolov VYu, Krivoruchko AV (2009) Orientation effects in 2–2 piezocomposites based on $(1-x)Pb(A_{1/3}Nb_{2/3})O_3-xPbTiO_3$ single crystals (A = Mg or Zn). J Appl Phys 105:074105–074107
38. Sessler GM (1981) Piezoelectricity in polyvinylidenefluoride. J Acoust Soc Am 70:1596–1608
39. Zhang R, Jiang B, Cao W (2003) Single-domain properties of $0.67Pb(Mg_{1/3}Nb_{2/3})O_3 - 0.33PbTiO_3$ single crystals under electric field bias. Appl Phys Lett 82:787–789
40. Poizat C, Sester M (2001) Homogénéisation périodique de composites piézoélectriques 0–3: influence de la distribution. Rev Compos Matér Av 11:65–74